Micro-vortex Generator (MVG) for Scramjet Inlet Application

Azam Che Idris, Mohd Rashdan Saad* and Konstantinos Kontis***
**National Defence University of Malaysia (NDUM)*
Sungai Besi Camp, 57000, Kuala Lumpur Malaysia
***University of Glasgow*
Glasgow, G12 8QQ, Scotland, United Kingdom

Abstract
Global measurement approach in characterizing a generic scramjet inlet has enabled investigation of various flow phenomena typically occurred on an inlet to be investigated further. This paper examines the effectiveness of MVG array in suppressing boundary layer separations on such an inlet. Global measurement of pressure and temperature were employed to visualized vortex pairs emanating from the MVG. The global pressure map showed the benefit of lower re-attachment peak pressure that usually accompany the large separation bubble at a scramjet inlet throat.

1. Introduction

Comprehensive global measurement of flow on a generic scramjet inlet-isolator has been demonstrated by Idris *et al.*[1]. They showed that it was possible to apply highly sensitive, platinum-based, Pressure Sensitive Paint (PSP) onto the external and internal surface of a scramjet inlet in Mach 5 and produce amazing flow topology with rich quantitative information. Their techniques open up new opportunities to fully understand different complex flow phenomena that exist on a scramjet inlet. This paper aims to replicate their techniques in order to investigate the mechanism of flow separation control using micro vortex generator in scramjet inlet application.

In our case, we observe the separation at compression corner between first and second ramp, and another at the inlet shoulder. Peculiarly, the re-attachment along with the decay of streamwise vortices/Goertler vortices on the second ramp could help in ensuring turbulent boundary layer flowing into isolator section, thus preventing the separation at shoulder. Nonetheless, it has been reported by Nguyen *et al.*[2] and Reinartz *et al.*[3] that flow 'relaminarization' could occur due to pressure drop and acceleration of flow at expansion corner (inlet shoulder). Following the example from Reinartz *et al.*[3], vortex generator is placed on the second ramp to control shoulder separation. Contrary to their study, MVG array are utilised in this study to achieve the same effect. The MVG array was shaped from strip of sand paper and the effectiveness three different grade of sand paper are discussed in the next section.

2. Methodology and Experimental Setup

2.1 High Supersonic Wind Tunnel

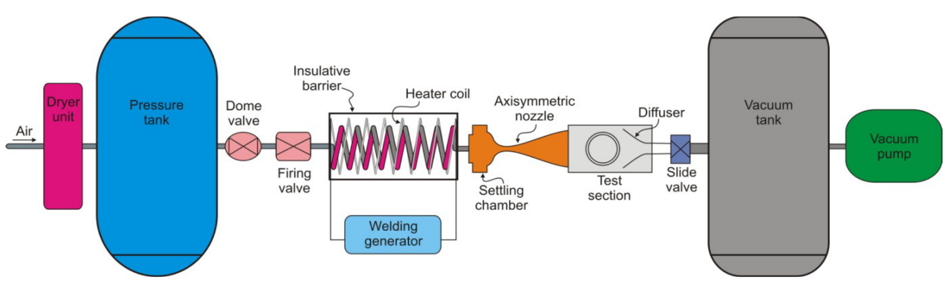

Figure 1: High supersonic tunnel in The University of Manchester

All experiments reported in this paper were conducted in the blowdown High Supersonic Wind Tunnel (HSST) in The University of Manchester, United Kingdom such as shown in Figure 1. The tunnel operates using compressed air stored at 16 bar. The total pressure was set at 645 kPa using the Type C4 model 208/3 dome valve.

Heating of the working fluid is provided by 24 kW direct current electric resistive heater. The stagnation temperature was about 370 K. The axisymmetric nozzle is changeable between Mach 4, Mach 5 and Mach 6. All experiments were conducted using Mach 5 nozzle as the generic scramjet inlet model was designed to operate at said flow speed.

2.2 Pressure Sensitive Paint (PSP) Measurement

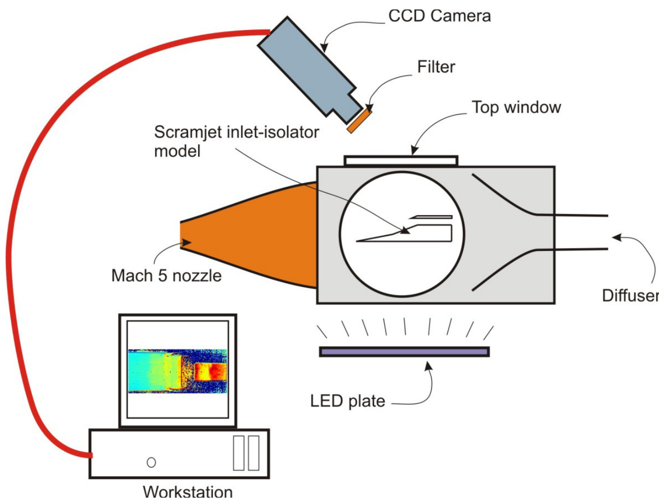

Figure 2: Side view of PSP system Setup for compression ramps and isolator surface pressure measurement

Figure 2 shows the side view of PSP system Setup optimized for measuring pressure intensity on compression and body-side isolator surface. The camera was placed on top of the test section, with its lens focused onto the model through the top window at an angle. The camera setup angle was not important because model length was calibrated by markings on the model. The angle of camera placement was adjusted as necessary to accommodate the full model length. The scramjet inlet-isolator model was fixed on sting holder, which can be rotated on horizontal-vertical plane to vary the model angle-of-attack. For this setup, LED plates were placed on both side windows for even illumination on the model. LED lamps were preferred than other light source due to their monochromatic nature. Filter was used for the camera to minimize recording of unwanted photon from environment. For in-situ calibration, static pressure distribution was measured using discreet transducer at the same time as pressure intensities were recorded. Intensity measurements were done in the darkest possible condition to reduce light contamination.

Scientific grade 12 bit CCD camera model LaVision Imager Intense was used as the main photon detector device for both setups. The camera was set to optimum exposure time of 7.5 ms with frame rate of 10 Hz. Sufficient exposure time was needed to allow the camera to capture the maximum photons possible and make use of its full-well capacity. Recorded images were pre-processed and viewed in real time by using Davis 7.0 software installed on Microsoft Windows-based workstation connected to the camera. MATLAB image processing toolbox was then utilised for further data processing.

2.3 Infrared (IR) Measurement

FLIR ThermaCAM SC 3000 Infrared camera was available for current experiments. The images can be captured with frequency of up to 900 Hz in 14-bit format. For current experiments, the camera was set to capture only 100 Hz. Its thermal sensitivity was 20 mK at standard temperature of 30 ^{0}C. It can automatically correct for different atmospheric conditions based on distance, temperature and relative humidity. ThermaCAM Researcher Software was used to process in real time the raw image captured by the camera.

The camera was placed on top of test section similar to PSP setup. This was because only top plate can be fitted with germanium window required for IR measurement. The model was painted black to achieve emissivity of about 0.95. As the material of scramjet inlet-isolator is made from aluminium which has high heat conductivity, measurement of heat transfer would not be shown. Instead, vortex formation, if any, would be visualized by delta-temperature map taken every two seconds. The schematic of the experimental setup is shown in Figure 3 below:

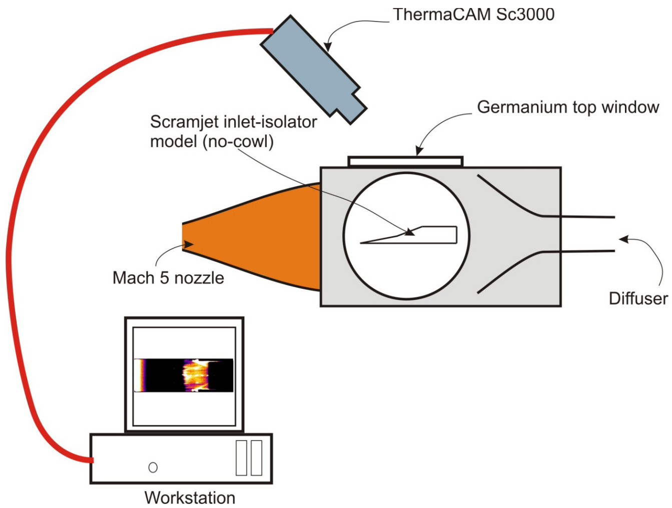

Figure 3: Schematic of IR thermography experimental setup

3. Roughness-Induced Transition for Suppressing Compression Corner Separation

Exploratory study of boundary layer trip using sand paper strip has been done on the compression ramp at Mach 5 with no angle-of-attack (AoA). Three sand paper strip of grit size P60, P100 and P150 has been selected for this study. They were cut into strip of size 5 mm × 36 mm. Their location on the first ramp was selected by considering the requirements of having low boundary layer edge Mach number and thick enough boundary layer to accommodate the strip[4]. The location selected is x/L = 0.12 where the local boundary layer thickness was found to be of 0.7 mm (see Figure 4). The strip was pasted onto the aluminium surface using double-sided tape of thickness 0.08 mm where the leading edge of the roughness strip was aligned at the x-coordinate selected. The results for different case are presented in Table 1 below:

Table 1: Location of transition starting point for different grade of sand paper

Case	Total strip height (mm)	Mach Number	Unite Reynolds Number	Transition (x/L)
P150-strip	0.28	5 ± 0.4%	13.2×10^6 m^{-1}	none
P100-strip	0.43	5 ± 0.4%	13.2×10^6 m^{-1}	0.30
P60-strip	0.65	5 ± 0.4%	13.2×10^6 m^{-1}	0.26
MVG-array	0.65	5 ± 0.4%	13.2×10^6 m^{-1}	0.23

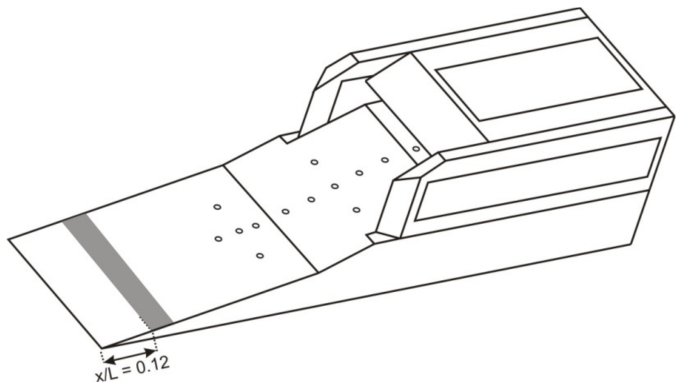

Figure 4: Position of sand-paper strip from leading edge

Processed schlieren images (not shown in this paper) indicate that P150-strip case was not able to affect the compression corner separation. The boundary layer edge was clearly visible up to the separation point. With P100-strip case, the flow transitioned to turbulence at x/L = 0.3 while the flow still separates at the compression corner. The separation shock was barely visible and the re-attachment shock moved closer to compression corner. Further increasing the roughness size in P60-strip case, the separation at compression corner was fully eliminated and the transition onset point moved further upstream (x/L = 0.26).

3. MVG-Induced Transition for Suppressing Compression Corner Separation

The effectiveness of P60-strip case in eliminating compression separation has made it as a suitable candidate for exploratory study on MVG in scramjet inlet-application. Roughness element of P60-strip case has been cut into a vortex generator array of three connected triangular vortex generator. Each vortex generator has spanwise length of 7 mm and streamwise length of 5 mm such as shown in Figure 5. This corresponds to hypotenuse length of, c = 6.1 mm for each single MVG. The half apex angle was set to be A = 35^{o}. The height of the vortex generator is similar to P60-strip element thickness of h = 0.65 mm. The dimension was chosen for purely convenient reason, which does not place too much importance in optimum shape of the MVG. This was due to this experiment being exploratory in nature thus any possibility in optimization was reserve for future studies. Three single MVGs were positioned together into an array with distance between every apex was set to s = 7 mm (see Figure 6). Its shape is similar to prism-type used in paper by Schulein and Trofimov[5] albeit with roughness effect included on its surface. Its spanwise location was set by aligning the centerline of MVG array to coincide with model centerline. The x-coordinate of MVG array was located at 15 mm from inlet leading edge so as to increase the percentage of vortex generator height to local boundary layer height and to ensure maximum effectiveness of MVG (see Figure 7).

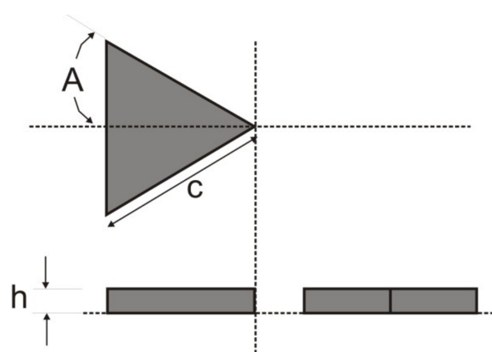

Figure 5: Dimension of a single MVG

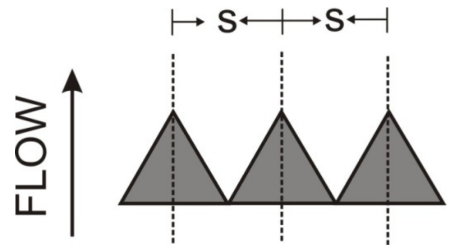

Figure 6: Distance between MVGs in an array

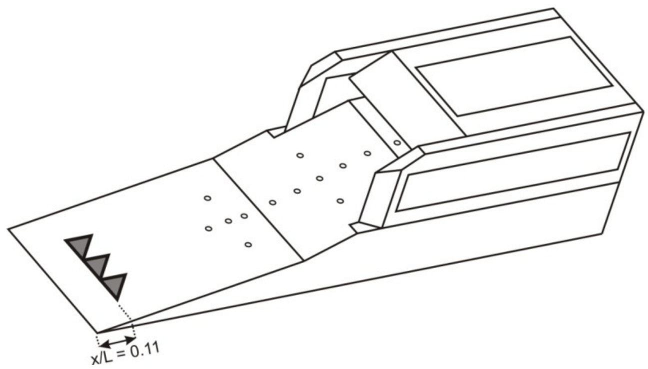

Figure 7: The MVG array was positioned with distance, x/L = 0.11, from leading edge and its middle apex coincide with inlet centreline

Processed schlieren images (not shown in this paper) indicate the effectiveness of the MVG in eliminating the compression corner separation. The transition region for MVG case was more upstream or at least comparable to that for P60-strip case (see Table 1). Besides the formation of turbulence, the MVG also promoted the formation of horseshoe vortex (see Figure 8) that may add towards the elimination of compression corner separation.

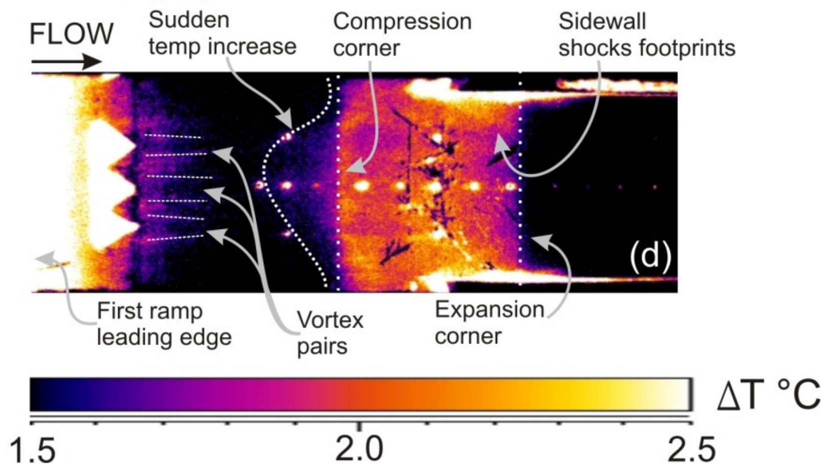

Figure 8: Horse-shoe vortex pair created by each MVG in the array as shown by delta-temperature map from IR thermography

4. MVG-Induced Transition for Suppressing Expansion Corner Separation

Eventhough MVG-array has been able to control compression corner separation by inducing turbulent early on the first ramp, expansion corner re-laminarization means that boundary layer separation could still occur. With that in mind, the MVG array has been re-positioned to the middle of second ramp to test its effect in suppressing shoulder separation. Reinartz *et al.*[3] have demonstrated the way to minimize the extent of shoulder separation by placing boundary layer trip device on the compression surface closest to expansion corner without detail quantitative analysis. In this current study, the PSP technique has been applied to quantitatively characterize the isolator flow in the present of MVG array. The MVG array was positioned at the middle of second ramp to avoid its interaction with re-attachment shock just upstream of that location (see Figure 9).

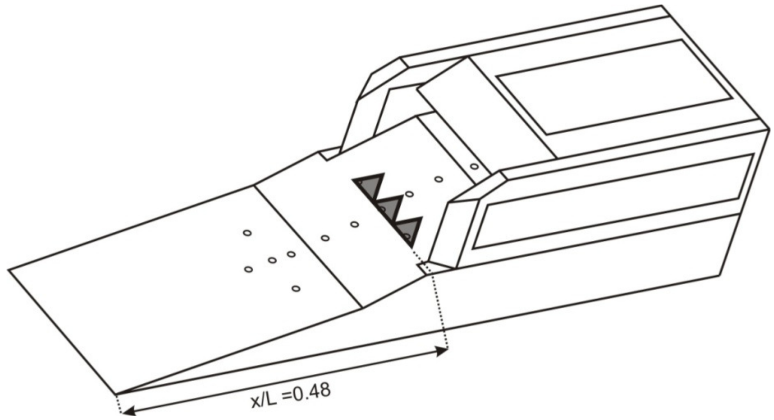

Figure 9: The MVG array was positioned with distance, x/L = 0.48, from leading edge and its middle apex coincide with inlet centreline

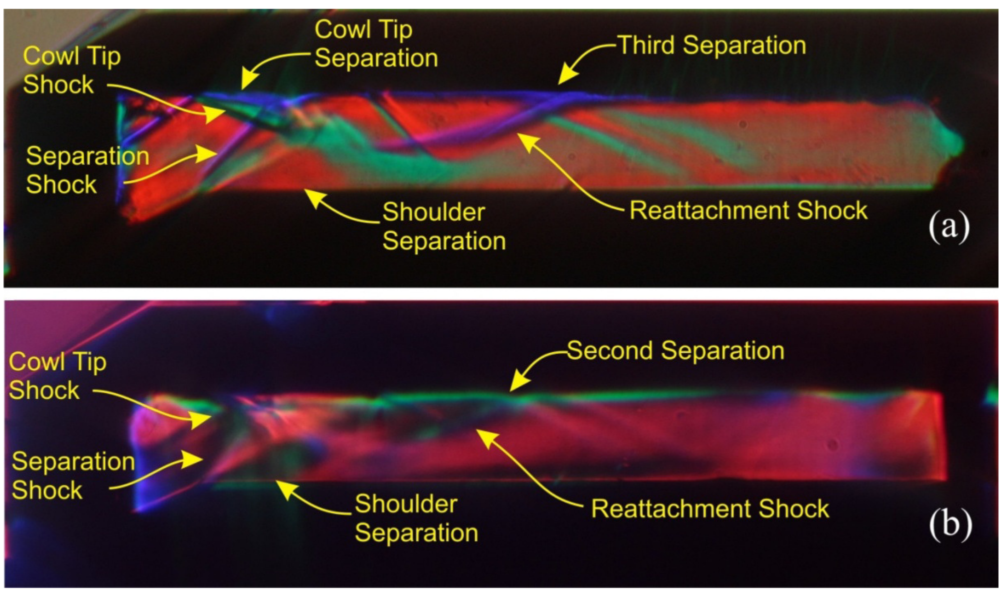

Figure 10: Experimental schlieren image of isolator flow for (a) Baseline (no-MVG) and (b) with MVG-array

Figure 10 shows the comparison of isolator shock structures of case without and with MVG. Shoulder separation still occurs in Figure A10(b) but with smaller size. Smaller shoulder boundary layer produced separation shock that was not strong enough to induce separation around cowl tip region like in Figure 10(a). The separation induced by shoulder re-attachment shock also appeared smaller in the MVG case. It was observed that the shock structures inside the isolator were faintly visible in MVG-array case, indicating that the shocks were mostly weak and there was a high level of flow uniformity.

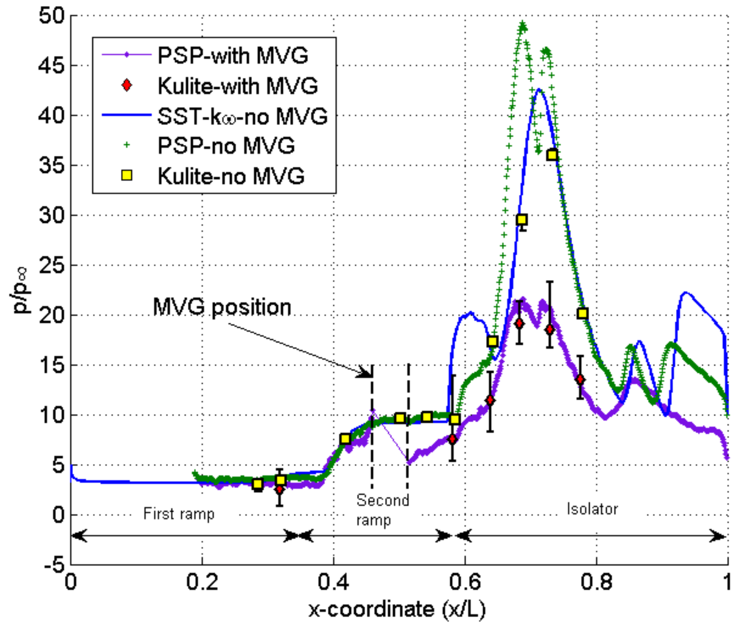

Figure 11: Normalized static pressure profile of without and with-MVG case

The pressure profile taken on the centerline of the model for Baseline and MVG case was compared in Figure 11. The intensity measured by the PSP camera was calibrated against Kulite readings distributed on both the internal and external part of the scramjet inlet. Significant oscillations in pressure were detected for all transducer locations downstream of MVG location. PSP calibration curve for MVG-array case was satisfactory with coefficient of determination value, R^2 = 0.976. Pressure predicted by PSP in unit bar was correct to within ± 0.048 (non-dimensionalized unit).

The pressure measured using PSP for MVG-array case was consistently lower than Baseline case, in the region downstream of MVG locations. The figure also shows that even though separation still occurs inside the isolator, severity of its re-attachment shock has dropped by more than 50%. The re-attachment peak pressure for MVG-array case also moved upstream, closer to shoulder. Subsequently all pressure peaks inside the isolator has been reduced as well.

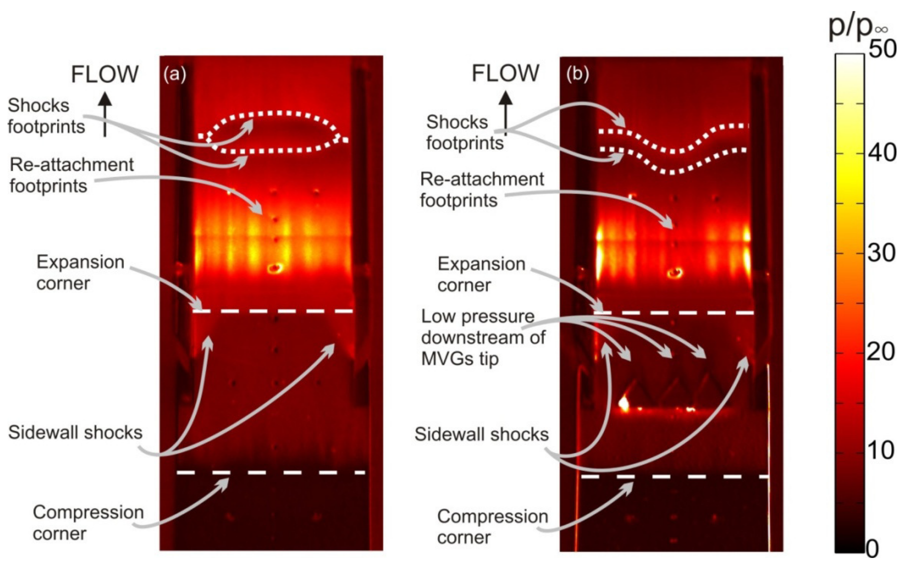

Figure 12: Inlet-isolator surface pressure comparison of no-MVG and with-MVG. Image is processed from raw PSP data

The three-dimensional effect of MVG on the flow is shown in Figure 12. On the second ramp surface, the pressure drop is confined only at a small streak downstream of each individual vortex generator. Similarly, the reduction in re-attachment pressure peak is also limited in the middle region which is under the influence of MVG, therefore resulting in the distortion of subsequent shock footprints further downstream.

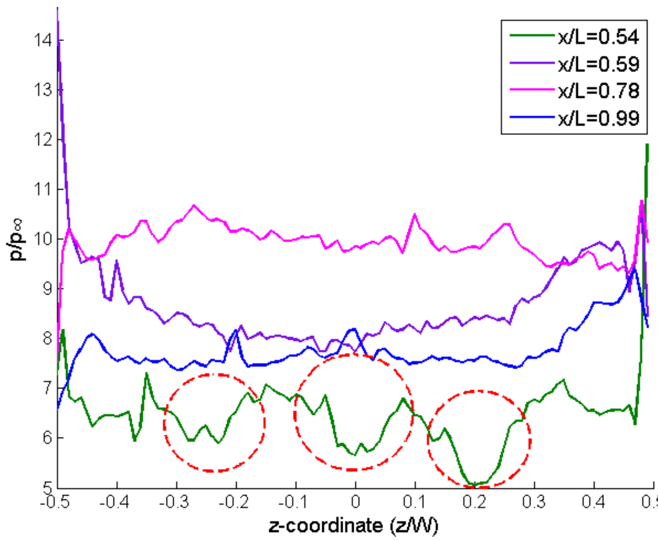

Figure 13: Spanwise pressure at different streamwise location for case with-MVG. Plot is processed from raw PSP data

Spanwise pressure has been taken at the start (x/L = 0.59), middle (coordinate x/L = 0.78) and end of isolator segment (coordinate x/L = 0.99) and compared in Figure 40. The spanwise pressure at position immediately downstream of MVG array (x/L = 0.54) has been included as well. The pressure drop associated with vortex streak emanating from each individual MVG has been detected (marked with red-dashed circle in Figure 13). This drop in pressure is followed by gradual pressure increase similar to observation made by Li and Liu[6] shown in Figure 14.

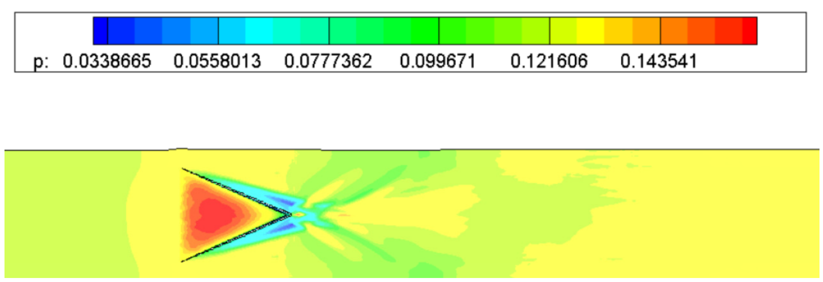

Figure 14: Typical pressure contour of flow on flat plate with a single MVG (flow from left to right) (figure taken from Li and Liu[6])

4. Conclusion

The MVG has proven itself as an effective counter-measure for mitigating boundary-layer separation. The mechanism of which it achieves that objective is by horse-shoe vortex formation that flow from downstream of the MVG. In scramjet inlet application, elimination of separation at shoulder improved the overall flow of the inlet. The structure of the inlet experienced much less impinging pressure from the boundary layer re-attachment that always come with the separation.

References

[1] Idris, A.C., Saad, M.R., Zare-Behtash, H., and Kontis, K. Luminescent Measurement Systems for the Investigation of a Scramjet Inlet-Isolator. *Sensors* **14**, 6606-6632 (2014).

[2] Nguyen, T., Behr, M., Reinartz, B., Hohn, O., and Gülhan, A. Effects of Sidewall Compression and Relaminarization in a Scramjet Inlet. *Journal of Propulsion and Power* **29**, 628–638 (2013).

[3] Reinartz, B.U., Herrmann, C.D., Ballmann, J., and Koschel, W.W. Aerodynamic performance analysis of a hypersonic inlet isolator using computation and experiment. *Journal of Propulsion and power* **19**, 868–875 (2003).

[4] Berry, S.A., Auslender, A.H., Dilley, A.D., and Calleja, J.F. Hypersonic boundary-layer trip development for Hyper-X. *Journal of spacecraft and Rockets* **38**, 853–864 (2001).

[5] Schülein, E., and Trofimov, V.M. Steady longitudinal vortices in supersonic turbulent separated flows. *Journal of Fluid Mechanics* **672**, 451–476 (2011).

[6] Li, Q., and Liu, C. Numerical investigations on the effects of the declining angle of the trailing-edge of MVG. *AIAA paper* **714**, 2010 (2010).